EARTHQUAKE ENGINEERING AND STRUCTURAL DYNAMICS, VOL. 25, 815-836 (1996)

A SIMPLIFIED METHOD FOR PREDICTION OF KINEMATIC SOIL–FOUNDATION INTERACTION EFFECTS ON PEAK HORIZONTAL ACCELERATION OF A RIGID FOUNDATION

S. K. SARMA AND M. SRBULOV

Department of Civil Engineering, Imperial College of Science, Technology and Medicine, Imperial College Road, London SW7 2BU, U.K.

SUMMARY

The kinematic soil–foundation interaction changes the free field ground motion to a different motion at the foundation of a structure. This interaction effect may be expressed by the ratio of the peak horizontal acceleration of a rigid and relatively lightweight foundation to the peak horizontal acceleration at the ground surface in the free field. It is found that the interaction effect can be defined by a simple function of the ratio of the peak horizontal ground velocity and ground acceleration in the free field, the length of the foundation and the shear wave velocity in the soil. Predictive equations for the kinematic soil foundation effect are derived using 350 strong motion records generated by 114 earthquakes world-wide. At the same time, an attenuation relationship is derived for the ratio of the peak horizontal ground velocity and acceleration from the same set of data. Ten case histories are studied; the interaction effects are calculated by using the predictive equations and then compared with measured field values. The results of the comparison illustrate the degree of predictive capability of the method when the foundation mass and the inertial soil–foundation interaction are not considered.

KEY WORDS: prediction; peak horizontal acceleration; rigid foundation

INTRODUCTION

The seismic ground motions recorded on the foundations of structures are usually different from those recorded in the free field. In general, when the foundation and the underlying soil is flexible, the combined response gives rise to a complex soil–foundation interaction. Simple solutions to this problem are not available. Only sophisticated analysis such as using radiating or transmitting boundaries in finite element methods can take some of this effect into account. If the foundation (structure) is very rigid compared to the underlying foundation soil then the rocking motion of the foundation may appear, which will affect the characteristics of the foundation motion . The limited shear strength of soil may also cause sliding of the foundation block. This sliding will also alter the characteristics of the foundation motion compared to the free field.

In addition to the inertial soil–foundation interaction due to the existence of foundation (structure) mass, the size and stiffness of the foundation may also alter the foundation motion. If the seismic waves travel vertically upward while the foundation is horizontal, then all points of the foundation and ground in the free field are subjected to the same motion at any instant. But if the seismic waves travel in an oblique direction then ground motion in the free field will vary spatially at a time. The rigid foundation cannot accommodate such variability. The foundation block will average out the variable input motion and the structure will be subjected to this average motion of the block. The averaging process will depend on the size of the foundation block in the direction of travel of the waves and on their velocity. The effect of the size of the rigid foundation is termed the kinematic soil–foundation interaction.

Most foundation analyses do not take kinematic soil–foundation interaction into account with the assumption of vertically propagating seismic waves. The foundation is assumed to be rigidly connected to the

CCC 0098–8847/96/080815–22

Received 7 December 1995
Revised 22 March 1996

base and the seismic input motion in the free field is applied at the base of the foundation. Much of the uncertainty in the estimation of soil–foundation interaction effects is due to unknown seismic loading but also –due to the variability of soil properties and complex foundation response. For practical applications, the estimation of the effects of soil–foundation interaction must be simple and involve design variables that can be assessed by the engineer, *a priori*, with some confidence. The introduction of additional variables describing the complex problem, on the other hand, may improve the prediction but this will put the onus on the selection of the appropriate values for these additional variables.

Yamahara[1] reported a reduction in the amplitude of the motions in the high-frequency range of large rigid foundations and suggested a simplified procedure in the frequency domain for estimating the effective translational input motion for response calculations of buildings. Scale model tests[2] and a number of field measurements in the U.S.A and in Japan (see the case histories in Appendix II) have shown a significant effect of soil–foundation interaction in reducing the peak acceleration of foundations compared to the free field. On the other hand, amplification of peak ground acceleration in the foundation of a structure compared to the free field is also known in buildings[3,4], which may be due to the resonant inertia effect of the structure.

Newmark[5] developed a rational basis for determining torsional earthquake effects in symmetric buildings arising from earthquake wave motions. More rigorous analyses for surface foundations of rectangular shape and various angles of incidence of seismic waves are also available.[6–8]

Peak ground acceleration is traditionally used as a single parameter for the earthquake resistant design of structures. Even though the suitability of peak ground acceleration as a simple measure of the damage potential of an earthquake is often questioned and other more rational parameters are sought[9,10] peak acceleration continues to be used as, for example, to anchor a standard spectral shape to the design value of zero period acceleration as in Eurocode 8 and in other design codes. When complex soil–structure interaction solution is not required, the peak acceleration is usually specified at the foundation level of a structure and is given as the free field motion.

APPLIED NUMERICAL AVERAGING TECHNIQUE

Ground acceleration at a site near the source is mainly induced by incident body shear waves inclined at an angle to the horizontal. At longer distances, these combine with other types of seismic waves. Because of inclined incidence, all points of ground in the free field are not subjected to the same acceleration at an instant. Spatial variation of ground acceleration cannot be accommodated by a rigid foundation, which can only be subjected to an averaged (resultant) acceleration over the foundation area. Newmark *et al.*[11] proposed a simple numerical model for averaging ground accelerations over a rigid footing. In this paper, a similar approach with some modification is used.

If there is no relative displacement between rigid foundation and ground underneath and the foundation mass is uniformly distributed then the expression for the average translational acceleration $a_{s,t}$ of a rigid foundation at time t is: (see Figure 1)

$$a_{s,t} = \frac{1}{L_s}\int_{L-L_s}^{L} a_l \, dl$$

$$= \frac{V_s}{L_s}\int_{t-T_s}^{t} a_t \, dt$$

$$= \frac{1}{T_s}(v_t - v_{t-T_s}) \tag{1}$$

where L_s is the length of the foundation in the direction of propagation of the wave front, L is the distance of the farthest edge of the foundation from a reference point located outside the foundation area, a_l is the ground acceleration at distance l along the foundation at time t, V_s is the velocity of propagation of seismic waves and is assumed equal to the velocity of shear waves passing through the ground beneath the

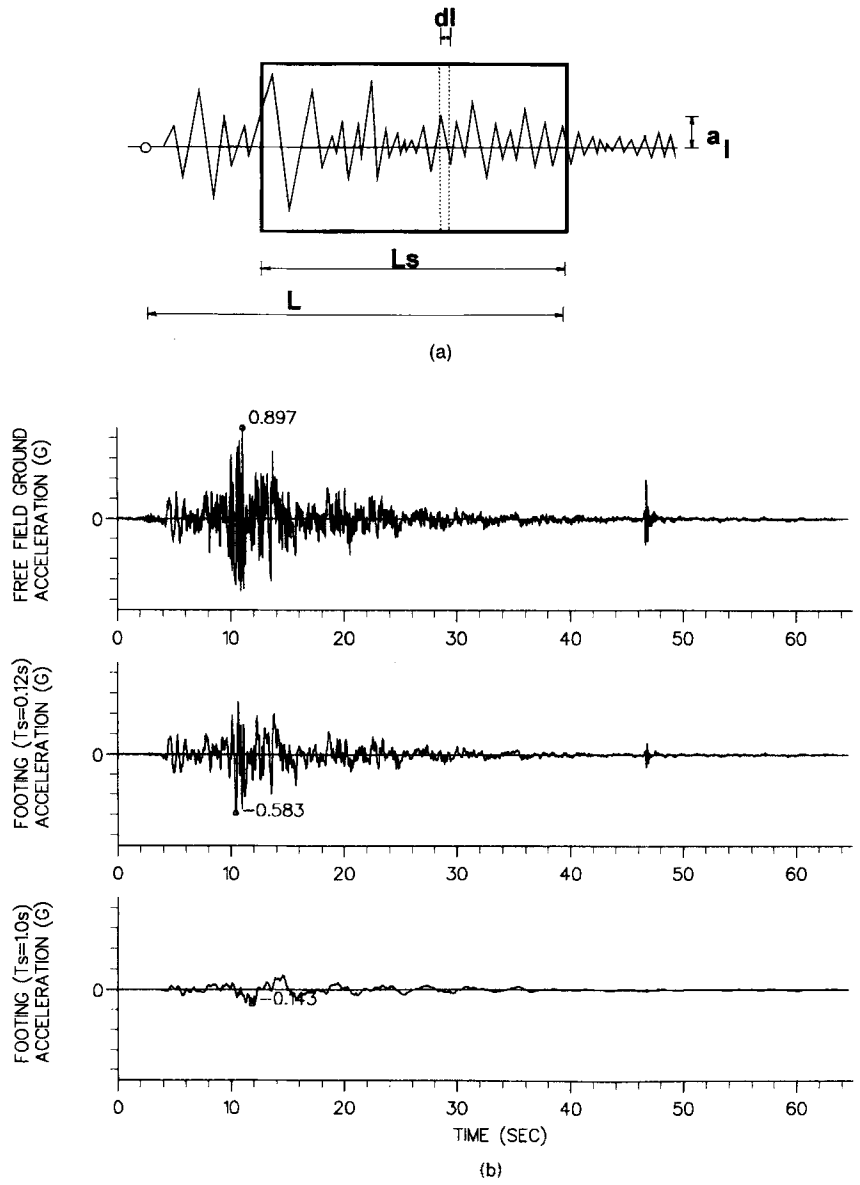

Figure 1. (a) Computational model for $a_{s,t}$ from equation (1). (b) An example of computation of $a_{s,t}$ showing the input data (ground acceleration time history) and the results of the computation for the footing with T_s = 0·12 and 1·0 s

foundation, v_t, v_{t-T_s} are the ground velocities at times t and $t - T_s$. T_s is the time (in s) necessary for a seismic wave to pass beneath the foundation. Because it is difficult to determine the length of the path of seismic waves beneath the foundation it is assumed that the travelling length of seismic waves is equal to L_s and that $T_s = L_s V_s^{-1}$ with a possible similar margin of error caused by the assumption about V_s. Near the beginning of an acceleration record when $t < T_s$, v_{t-T_s} should be replaced by v_0 (initial ground velocity) and near the end of the record when $t > t_{end}$, v_t should be replaced by v_{end} (final ground velocity). The maximum value of t is $t_{max} = t_{end} + T_s$.

The average acceleration is assumed to act in the middle of the foundation. However, due to the non-uniform distribution of ground acceleration over the foundation at any instant, the resultant

acceleration does not act at the centre of the foundation. The offset from the centre of the foundation can be expressed by the eccentricity, which is a function of time (see Appendix I). As a result of this eccentricity, the accelerations away from the centre will be different from the average value. Newmark[5] gives the value of the eccentricity at about 5–10% of the length of the foundation. The calculations, as shown in Appendix I, give a similar range of values but the prediction of the eccentricity is uncertain due to the large scatter of the computed values and is therefore not used for the case histories.

In order to obtain a predictive relationship between the average foundation acceleration and earthquake source parameters, a suite of ground acceleration records and a range of values of T_s are selected. These values of T_s are 0·04, 0·12, 0·24, 0·48 and 1·0 s.

SELECTION OF GROUND ACCELERATION RECORDS

The data set consists of 350 biaxial components in the horizontal direction of ground acceleration time histories generated by 114 earthquakes worldwide (Table I). The surface wave magnitudes of these events range from 4 to 7·7, and source to site distances range from 0 to 200 km. The smallest peak ground acceleration is 0·01 g and the maximum 1·34 g. Figure 2 shows the distributions of earthquakes and records in the data set in terms of magnitude, depth, distance and peak acceleration.

Table I. Basic data of the earthquakes and records

Date	O.T.	h	M	$\log(M_0)$	Q	No. R	Range d	Country
1938 9 12	0610	10	5·6			1	27	USA
1940 5 19	0436	7	7·1	26·59	S	1	9	USA
1941 7 1	0750	15	5·7	24·95		1	12	USA
1941 10 3	1613	10	6·5			1	29	USA
1949 3 9	1228	10	5·2		T	1	20	USA
1951 10 8	0410	10	6·0			1	41	USA
1952 7 21	1152	16	7·7	27·30	T	4	42–109	USA
1954 12 21	1956	15	6·7	25·48	S	1	29	USA
1957 3 22	1944	7	5·3	23·87	T	1	11	USA
1961 4 9	0723	10	5·8		S	2	20	USA
1966 6 28	0426	7	6·1	25·36	S	7	6–105	USA
1968 4 9	0228	8	7·1	26·31	S	4	45–213	USA
1968 5 25	2349	12	5·4			1	24	NZL
1968 6 14	1903	15	5·4			1	28	NZL
1968 11 1	0132	20	5·5			3	32–42	NZL
1970 9 12	1430	8	5·5	24·00	T	7	15–110	USA
1971 2 9	1400	8	6·6	26·11	T	19	3–168	USA
1972 1 25	2025	5	4·1		N	1	13	ITA
1972 1 25	2322	10	4·0		N	1	9	ITA
1972 2 4	0242	8	4·4		SN	1	5	ITA
1972 2 4	0918	8	4·3		SN	1	16	ITA
1972 2 4	1719	2	4·2		SN	1	16	ITA
1972 2 4	1817	10	4·0		N	1	12	ITA
1972 2 5	0126	10	4·2		SN	1	3	ITA
1972 2 6	0134	4	4·1		SN	1	11	ITA
1972 2 8	1219	12	4·0		N	2	11	ITA
1972 6 14	1855	8	4·5		SN	1	8	ITA
1972 6 14	2101	8	4·0		N	1	1	ITA
1972 12 23	0629	5	6·2		S	1	5	NIC
1973 2 21	1442	12	5·6			1	27	NZL
1973 11 4	1552	7	5·7		T	1	11	GRE
1973 11 4	1611	15	4·6		T	1	14	GRE
1974 1 29	1512	13	4·1		N	1	12	GRE

Table I (*Contd.*)

Date	O.T.	h	M	$\log(M_0)$	Q	No. R	Range d	Country
1975 6 7	0846	6	5·6			5	6–60	USA
1975 8 1	2020	10	5·7	24·93	N	1	8	USA
1975 11 29	1447	11	7·1			1	27	USA
1976 5 6	2000	6	6·5	25·53	T	1	92	ITA
1976 5 17	0258	10	7·1	26·26	T	1	3	SSR
1977 12 29	1652	10	4·6			1	63	GRE
1978 8 13	2254	9	5·7	24·82	T	1	3	USA
1978 9 16	1535	5	7·3	27·11	T	3	3–34	IRN
1979 4 9	0210	13	5·2	24·18	T	2	17–30	YUG
1979 4 11	1214	15	4·5			1	19	TUR
1979 4 15	0619	12	7·0	26·49	T	4	9–65	YUG
1979 4 15	0631	10	4·8			1	52	YUG
1979 4 15	1243	6	4·0			1	7	YUG
1979 4 15	1443	7	5·8	24·78	T	2	22–42	YUG
1979 4 16	1004	11	4·9			2	3–81	YUG
1979 5 14	0953	5	4·2			1	7	YUG
1979 5 24	1723	5	6·3	25·34	T	2	18–30	YUG
1979 7 18	1312	5	5·0	24·04	N	1	6	TUR
1979 8 2	1441	5	3·9			1	16	YUG
1979 8 6	1705	6	5·7	24·78	S	6	1–9	USA
1979 10 15	2316	8	6·9	25·82	S	32	1–49	USA
1980 1 24	1900	12	5·9	24·79	S	1	16	USA
1980 11 23	1834	10	6·9	26·40	N	15	8–135	ITA
1981 1 16	0037	7	5·0	23·93	N	1	15	ITA
1981 2 14	1727	10	4·5			2	17–33	ITA
1981 2 24	2053	10	6·7	25·95	N	2	4–13	GRE
1981 2 25	0235	8	6·4	25·58	N	1	24	GRE
1981 3 10	1516	10	5·2			2	7–21	GRE
1981 4 10	0833	10	4·3			1	15	GRE
1981 5 25	2304	15	4·0			1	7	GRE
1981 5 27	1504	15	4·8			1	11	GRE
1983 1 17	1241	14	7·0	26·36	T	2	23–87	GRE
1983 3 16	2119	25	4·7			1	16	GRE
1983 3 23	1904	25	4·9			1	26	GRE
1983 3 23	2351	3	6·1	25·34	S	1	70	GRE
1983 4 16	2129	12	5·2			1	18	NZL
1983 5 2	2342	7	6·6	25·66	T	46	8–69	USA
1983 7 5	1201	7	6·0	25·26	S	1	55	TUR
1984 4 24	2115	8	6·2	25·41	S	17	4–79	USA
1984 5 7	1749	8	5·8	24·89	N	3	12–52	ITA
1984 5 11	1126	16	4·1	23·15		1	10	ITA
1984 5 11	1041	8	5·3	24·30	N	1	19	ITA
1984 5 11	1639	17	4·4	23·30	N	1	9	ITA
1984 10 25	0949	11	4·7			1	2	GRE
1985 8 31	0603	15	4·7			2	13–21	GRE
1985 12 23	0516	6	6·8	26·28	T	3	8–24	CAN
1986 9 13	1724	7	5·8	24·99	N	1	5	GRE
1986 10 10	1749	7	5·4	24·67		3	4–5	SAL
1987 3 2	0142	8	6·5	25·81	N	1	9	NZL
1987 5 14	0629	9	4·1			1	10	GRE
1987 10 1	1442	14	6·0	24·90	T	13	7–43	USA
1988 9 22	1205	12	4·4			1	28	GRE
1988 10 16	1234	12	5·6	24·88	T	1	28	GRE
1988 12 13	1100	5	4·0			1	20	GRE
1989 10 18	0004	17	7·2	26·66	T	27	1–98	USA
1989 10 29	1909	6	5·6	25·00	T	1	61	ALG

Table I (*Contd.*)

Date	O.T.	h	M	$\log(M_0)$	Q	No. R	Range d	Country
1990 2 19	0534	24	6·3	25·45	N	3	27–50	NZL
1990 5 13	0423	12	6·2	25·69	T	3	18–45	NZL
1990 5 17	0844	26	4·6			1	4	GRE
1990 6 16	0216	29	5·3	24·4		1	39	GRE
1990 8 8	0035	10	4·2			1	35	GRE
1990 12 21	0657	13	6·1	25·23	N	1	49	GRE
1991 1 28	1258	8	5·4	24·63	T	3	9–32	NZL
1991 1 28	1801	13	5·6	24·90	T	5	8–54	NZL
1992 3 13	1718	10	6·8	26·40	S	1	4	TUR
1992 3 15	1616	10	5·8	24·88		1	45	TUR
1992 5 30	1855	12	4·8			2	33–37	GRE
1992 11 18	2119	15	5·7			2	25–36	GRE
1993 3 26	1145	10	4·3			2	1–15	GRE
1993 3 26	1156	10	4·3			2	6–11	GRE
1993 3 26	1158	10	5·3			2	4–19	GRE
1993 3 26	1249	10	4·0			1	14	GRE
1993 6 13	2326	15	5·1			1	33	GRE
1993 7 10	2026	10	4·2			1	13	GRE
1993 7 14	1231	15	5·6			6	5–55	GRE
1993 9 26	0753	10	4·2			1	15	GRE
1993 11 4	0518	10	5·2			3	10–19	GRE
1994 1 14	0607	10	4·4			1	19	GRE
1994 2 25	0230	10	5·4			2	16–29	GRE
1994 2 27	2234	10	4·0			1	27	GRE
		10 (4·7)	5·4 (1·0)			350		

O.T. = origin time GMT
h = focal depth km
M = surface wave magnitude
M_0 = seismic moment (dyn cm)
Q = source mechanism; T: thrust, N: normal, S: strike-slip
No. R = number of biaxial components of time-histories used
Range d = range of horizontal site-source distances in km

The records come from instruments, mainly SMA-1 type accelerographs, located at the ground floors or in the basements of buildings and structures with up to three storeys and at free field sites regardless of topography. Sites have been classified as either 'rock' or 'soil' without regard to depth and shear wave velocity of deposits. The available acceleration time histories are of different levels of processing. Time histories were, therefore, base line corrected and low-pass filtered using an elliptic filter.[12] The corrected records were then used to compute the time histories of average accelerations, $a_{s,t}$ for various values of T_s from which the absolute maximum values A_s were picked out.

PREDICTIVE EQUATIONS AND REGRESSION RESULTS

Equation (1) can be used as a basis for the selection of the predictive equation for peak value A_s of $a_{s,t}$ as a function of T_s. It is clear that A_s is a function of the ground velocity and therefore the peak ground velocity, V_p, is considered as a parameter for curve fitting. Both A_s and V_p are normalized to the peak ground acceleration A_p. Due to non-linearity of this function and in order to be able to apply a linear regression analysis the predictive equation adopted for the influence of a rigid foundation on the attenuation of peak horizontal acceleration of the foundation is

$$\log(A_s/A_p) = C_1 + C_2 \log(V_p/A_p) + \sigma p \tag{2}$$

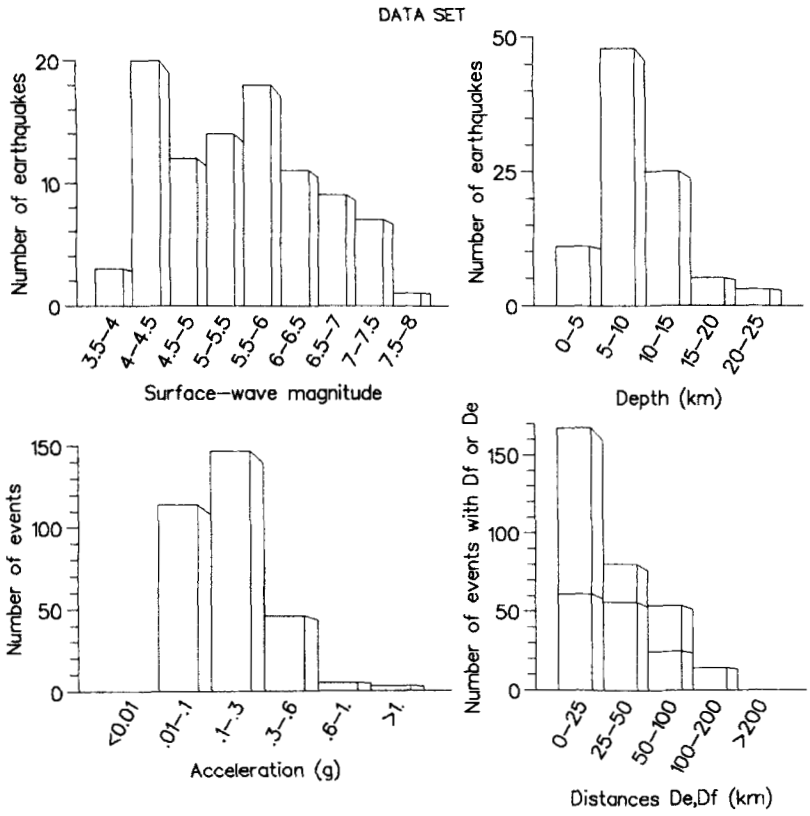

Figure 2. Data set distribution of earthquakes and associated records of horizontal acceleration with respect to surface-wave magnitude/depth and acceleration/distance respectively. The upper bars are for epicentral distances and lower for fault distances

where $p = 0$ applies for the mean and $p = 1$ applies for the 84 percentile value. Coefficients C_1 and C_2 are determined for values of $T_s = 0{\cdot}04$, $0{\cdot}12$, $0{\cdot}24$, $0{\cdot}48$, $1{\cdot}0$s. Standard deviation σ is about $0{\cdot}1$.

Values of C_1 and C_2 for different T_s ($0{\cdot}04$, $0{\cdot}12$, $0{\cdot}24$, $0{\cdot}48$, $1{\cdot}0$s) are shown in Figure 3. This shows that values of C_1 first increase with T_s and then slowly decrease while values of C_2 first increase with T_s and then remain nearly constant for larger values of T_s.

Figure 4 shows plots of the ratio (A_s/A_p) where A_s is calculated from the records using equation (1) versus the ratio predicted using equation (2) with $p = 0$. In the predictive equation, the values of (V_p/A_p) are also obtained from the records. From this figure it follows that ground type (soil or rock) does not affect the ratio and the scatter of the results. The stability of the results from the regression has been checked by regressing data in subsets formed from the data set. The results are not affected much by the sizes of the subsets and therefore the data set used can be considered as representative.

PREDICTION OF THE RATIO OF PEAK GROUND HORIZONTAL VELOCITY AND ACCELERATION

The ratio between peak horizontal ground velocity and acceleration can be obtained either by regressing directly on this ratio or by combining the two equations which individually predict peak horizontal velocity and acceleration. The latter approach is more general because individual acceleration and velocity predictions for peak values exist for different parts of the world. However, the use of such relationships derived from different sets of data may not be reliable.

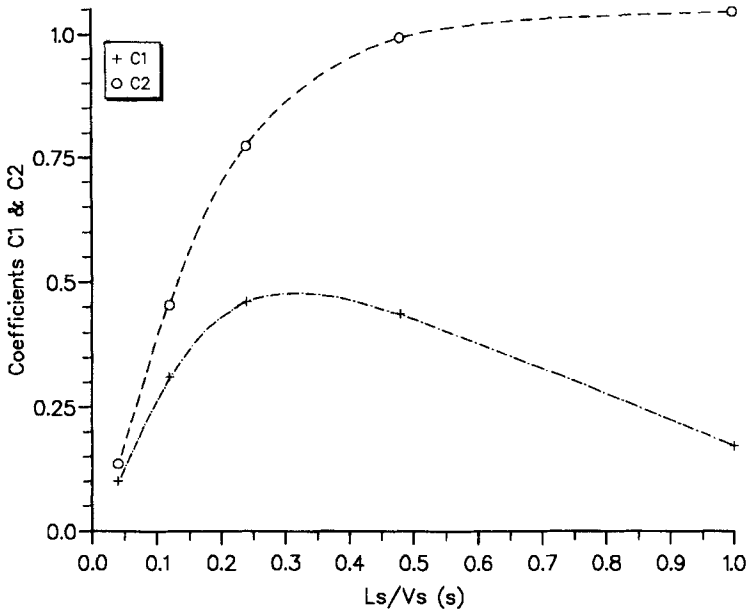

Figure 3. Values of coefficients C_1 and C_2 in equation (2) versus T_s

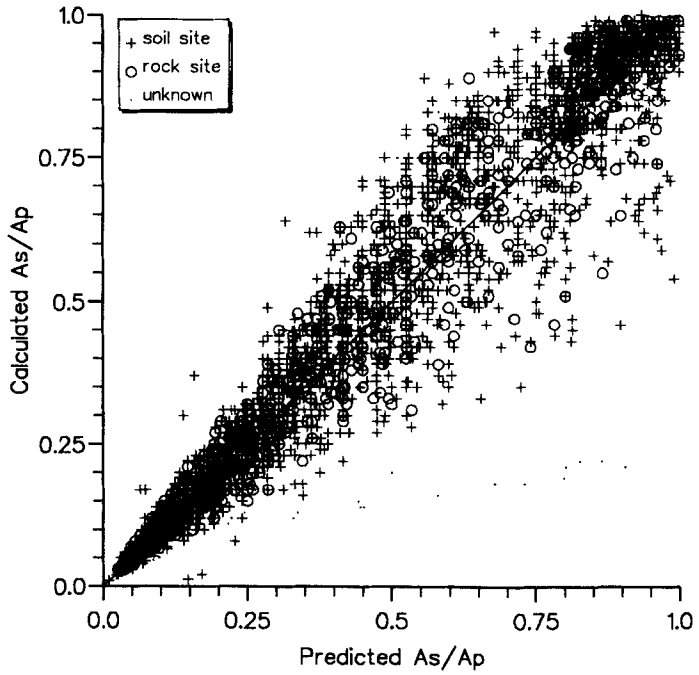

Figure 4. Calculated A_s/A_p from the records (equation (1)) versus predicted A_s/A_p from equation (2)

For the data set presented here, attenuation relationships are derived for peak horizontal ground acceleration A_p and peak horizontal ground velocity V_p. The regressions are performed using the two horizontal components as separate records in the first case and only the larger of the two components in the second case. For the attenuation relationship of (V_p/A_p), both the components are used. In this data set, M_s is

the surface wave magnitude, d is the closest distance to the projection of the fault rupture as defined by Joyner and Boore.[13] For smaller events or when fault distance is not available, epicentral distance is used. The distance parameter is given as $r = (d^2 + h_0^2)^{0.5}$. The constant h_0 accounts for the fact that the source of the peak motion is not the closest point on the surface projection of the fault rupture or the epicentral distance[13] and it does not represent explicitly the depth. The relationships are shown below.

Case 1: Both components included

$$\log(A_p/g) = -1{\cdot}617 + 0{\cdot}248M_s - 0{\cdot}5402\log r - 0{\cdot}00392r + 0{\cdot}26p, \quad r^2 = d^2 + 3{\cdot}2^2 \tag{3}$$

$$\log(V_p) = -0{\cdot}861 + 0{\cdot}432M_s - 0{\cdot}5692\log r - 0{\cdot}00270r + 0{\cdot}29p, \quad r^2 = d^2 + 2{\cdot}1^2 \tag{4}$$

$$\log(V_p/A_p) = -2{\cdot}117 + 0{\cdot}175M_s - 0{\cdot}0709\log r + 0{\cdot}00131r + 0{\cdot}19p, \quad r^2 = d^2 + 0{\cdot}7^2 \tag{5}$$

Case 2: Maximum component

$$\log(A_p/g) = -1{\cdot}507 + 0{\cdot}240M_s - 0{\cdot}542\log r - 0{\cdot}00397r + 0{\cdot}26p, \quad r^2 = d^2 + 3{\cdot}0^2 \tag{6}$$

$$\log(V_p) = -0{\cdot}750 + 0{\cdot}431M_s - 0{\cdot}6035\log r - 0{\cdot}00240r + 0{\cdot}30p, \quad r^2 = d^2 + 2{\cdot}0^2 \tag{7}$$

In these expressions, V_p is measured in cm/s and A_p is measured in cm/s^2.

If we derived the ratio (V_p/A_p) from equations (3) and (4) we would obtain

$$\log(V_p/A_p) = -2{\cdot}24 + 0{\cdot}184M_s - 0{\cdot}029\log r + 0{\cdot}00122r \tag{8}$$

which is nearly the same as that obtained from the original data but without the standard deviation and the constant term of the distant parameter becomes meaningless. However, the constants of the relationship show that consistent data yield consistent results.

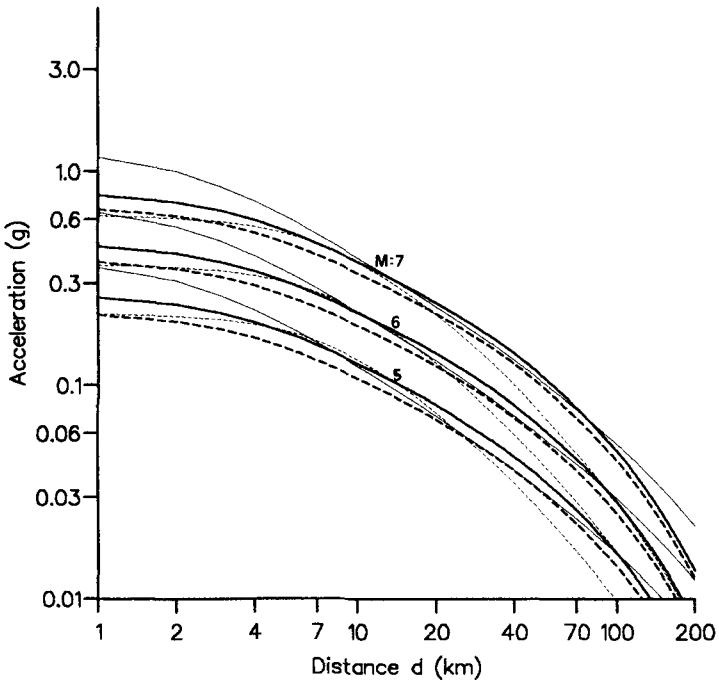

Figure 5. Predictive curves for mean peak ground acceleration as a function of magnitude values 5,6,7 and horizontal site–source distance d from equation (6)—thick solid line, equation (3)—thick dashed line, equation (9)—thin solid line and Joyner and Boore[15]—thin dashed line

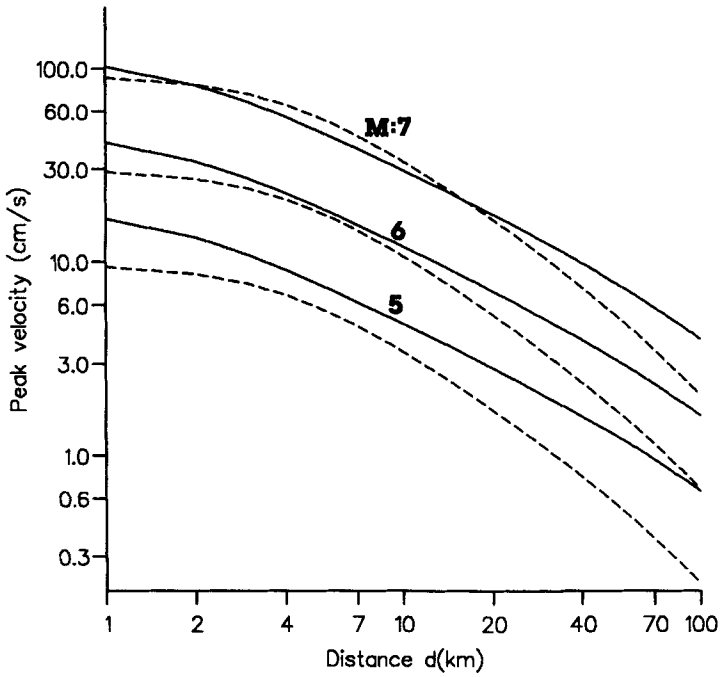

Figure 6. Predictive curves (solid lines) from equation (10) for mean peak ground velocity in Europe and adjacent regions as the functions of horizontal site to source distance d and surface wave magnitude values 5,6,7. Dashed lines are for the relationship from Joyner and Boore[15]

Ambraseys[14] derived predictive relationships for peak ground accelerations in the European area and adjacent regions using data from 1260 seismic events generated in free field or basement and ground floor of buildings with up to three storeys and at distances of up to 260 km. The events were generated by 619 shallow earthquakes, with depth less than 26 km, of magnitudes greater than 4. The predictive equation for ground peak horizontal acceleration without regard to local ground type is

$$\log(A_p/g) = -1{\cdot}43 + 0{\cdot}245M_s - 0{\cdot}0010r - 0{\cdot}786\log(r) + 024p, \quad r^2 = d^2 + 2{\cdot}7^2 \tag{9}$$

Equation (9) predicts the maximum value of the two horizontal components. In deriving equation (9) about 30 per cent of the peak accelerations were obtained from processed time histories with the rest from other sources. Figure 5 shows a comparison of the attenuation relationships derived here with that of Ambraseys[14] and Joyner and Boore.[15] The difference between equation (3) and equation (6) is obvious since the former represents both components while the latter is derived from the maximum of the two components. The difference between the other curves reflects differences in the data sets.

Ambraseys *et al.*[16] investigated the influence of local ground type on peak acceleration and found that expected values of the peak acceleration are about 25 per cent larger on soil sites than on rock sites, not an insignificant difference when compared with the standard deviation for a single prediction. Using this data set but ignoring records from distances greater than 100 km and using only the maximum of the two components, the predictive equation for peak ground horizontal velocity regardless of local ground type is derived which gives

$$\log(V_p) = -0{\cdot}553 + 0{\cdot}395M_s - 0{\cdot}00170r - 0{\cdot}717\log(r) + 0{\cdot}29p \tag{10}$$

where $r = (d^2 + 1{\cdot}6^2)^{1/2}$. The largest distance of 100 km was chosen because there were only a few records at greater distances and also to compare the results with those of Joyner and Boore.[15] Figure 6 shows both attenuation relations for comparison.

Table II. Complementary data for the case histories

No.	Reference	Country	Foundation	Ground	M	d	A_p
1	Valera *et al.*[21]	USA	Caisson	Dense sand	5·5	25	343
2	Hirashima *et al.*[22]	Japan	Deep raft	Rock	7·4	250	62
3	Kishida *et al.*[23]	Japan	Mat	Gravel	4·3	70	45
4	Tajimi *et al.*[25]	Japan	Thick slab	Dense sand	7·6	700	12
					5·5	33	24
					3·7	20	32
					5·4	10	41
5	Yajima *et al.*[26] and Ueshima *et al.*[27]	Japan	Mat	Sand, gravel	4·7	108	5
					5·5	116	18
					3·7	40	5
					6·1	56	34
					5·0	82	14
					4·5	75	7
					4·3	18	6
					4·2	58	7
					4·9	58	8
					3·6	27	5
					4·3	77	8
					6·1	50	51
					4·1	45	6
					4·5	57	4
					6·0	290	7
					3·9	26	9
					4·9	113	11
					4·9	141	10
					6·5	160	15
					4·8	7	28
6	Yamagami *et al.*[28]	Japan	Raft		7·9	705	24
7	Hirota *et al.*[29]	Japan	Spread		5·4	27	30
8	Osawa *et al.*[30]	Japan	Pad	Loam	4·5	50	4
					5·2	42	38
9	Hamada *et al.*[32]	Japan	Slab	Diluvium	7·6	510	2
10	Hamada *et al.*[33]	Japan	Shaft	Soft clay	6·9	600	5
					4·6	60	2

$M = M_L$ (U.S.A) otherwise Japanese scale
d = epicentral distance, km
A_p = measured peak acceleration in the free field (cm/s^2)

Combining equations (9) and (10) we get

$$\log(V_p/A_p) = -2{\cdot}115 + 0{\cdot}150M_s + 0{\cdot}069\log r - 0{\cdot}0007r \tag{11}$$

Comparing equations (5) and (11) we can see that the ratio (V_p/A_p) is mainly dependent on the magnitude of the earthquake. Equation (5) shows that the ratio decreases with distance in the very near source (< 25 km) and then increases slowly which is consistent with information about periods of strong motion records. Equation (11), on the other hand, shows an increase in the near field and then a decrease in the far field. From both equations, the effect of distance within about 100 km is small.

CASE HISTORIES OF MEASURED AND PREDICTED PEAK FOUNDATION ACCELERATION

Specific data for the case histories are given in Table II and in Appendix II. The predictions of peak ground velocity and acceleration with 50 per cent probability of exceedence for the case history from U.S.A. are

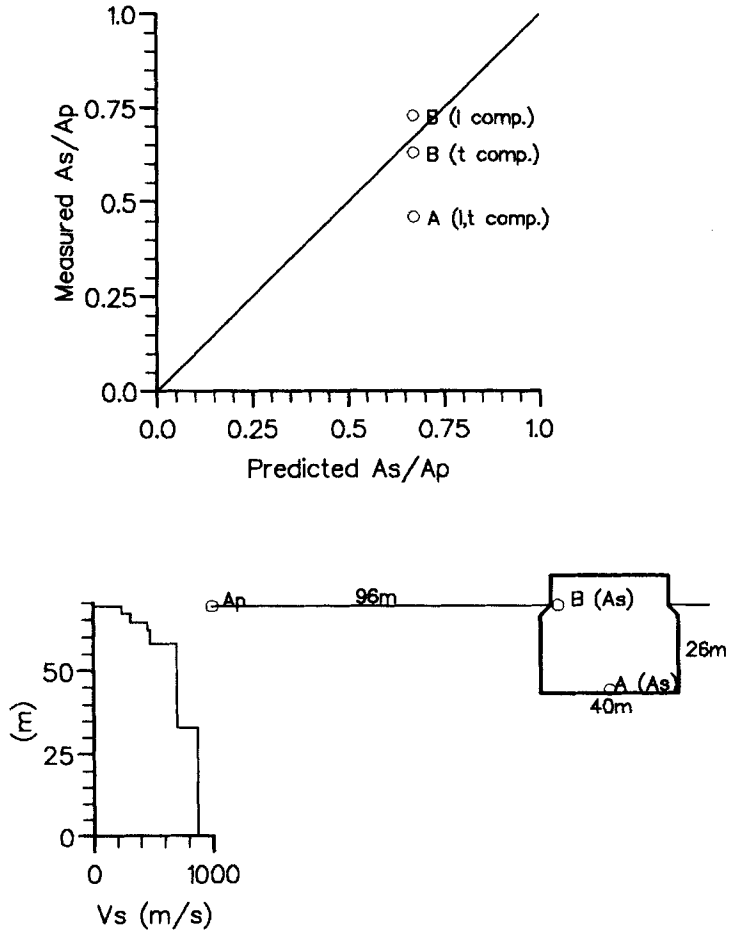

Figure 7. Relevant data for case 1: Humboldt Bay Power Plant

based on the equations from Campbell[17] while that for the case histories from Japan are based on the equations by Kawashima *et al.*[18]

A number of case histories for which the measurements of A_s and A_p indicated significant soil–structure interaction in seismic condition could not be considered due to insufficient data necessary for predictive equations. Also, case histories of the interaction for piled foundations have been excluded from consideration because ground shear wave velocities at the sites have been measured before pile installation. Installed displacement and bored piles cause an increase in bulk density and as a consequence of the shear wave velocity V_s. The increased velocity will cause , in turn, a decrease of T_s and an increase of A_s. Therefore, the predictions of A_s based on V_s measured without piles could be on the unsafe side.

DISCUSSION

It would be ideal to analyse both the inertial and kinematic soil–foundation interaction simultaneously. However, such complex analyses are rarely economically justified, except for very important structures and unusual foundation conditions. Therefore, in a simplified approach, the inertial and kinematic interactions are considered separately.

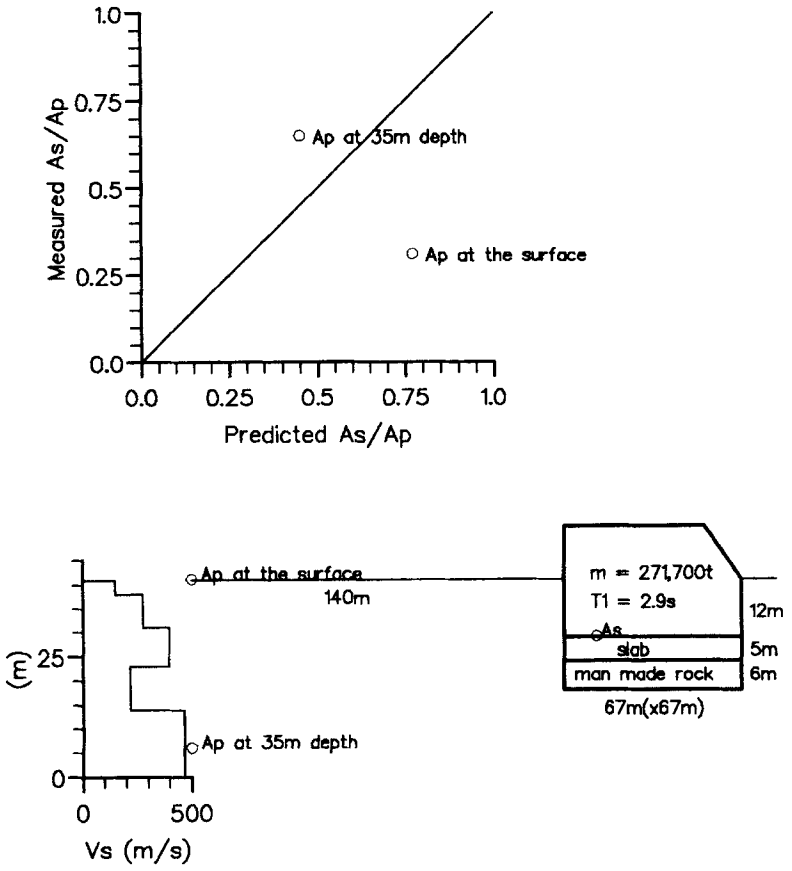

Figure 8. Relevant data for case 2: Tokai No. 2 Nuclear Power Plant

The prediction of peak foundation acceleration due to the kinematic interaction using the simplified method appears to be successful from the case studies. However, a number of factors, which may affect the results, need to be kept in mind.

(1) In the case of embedded foundations, the accelerations at the foundation level should be considered, rather than at the ground level.
(2) The horizontal acceleration of the foundation is affected by the eccentricity. The prediction of the eccentricity is rather difficult. However, its effect on peak foundation acceleration is small compared to the error associated with its prediction.
(3) Flexibility of the foundation causes the underprediction of peak foundation acceleration. The present method is valid for rigid foundations.
(4) Small sliding of the foundation with respect to its base can significantly reduce peak foundation acceleration. Ambraseys and Srbulov[19] showed that the design peak acceleration of the foundation may be reduced to the critical acceleration required to bring about sliding of the foundation. The critical acceleration is controlled by the yield resistance in undrained conditions.
(5) Non-uniform distribution of the foundation mass would induce greater rotational acceleration and will effect inertial soil–structure interaction, which is not considered in the simplified method presented here.

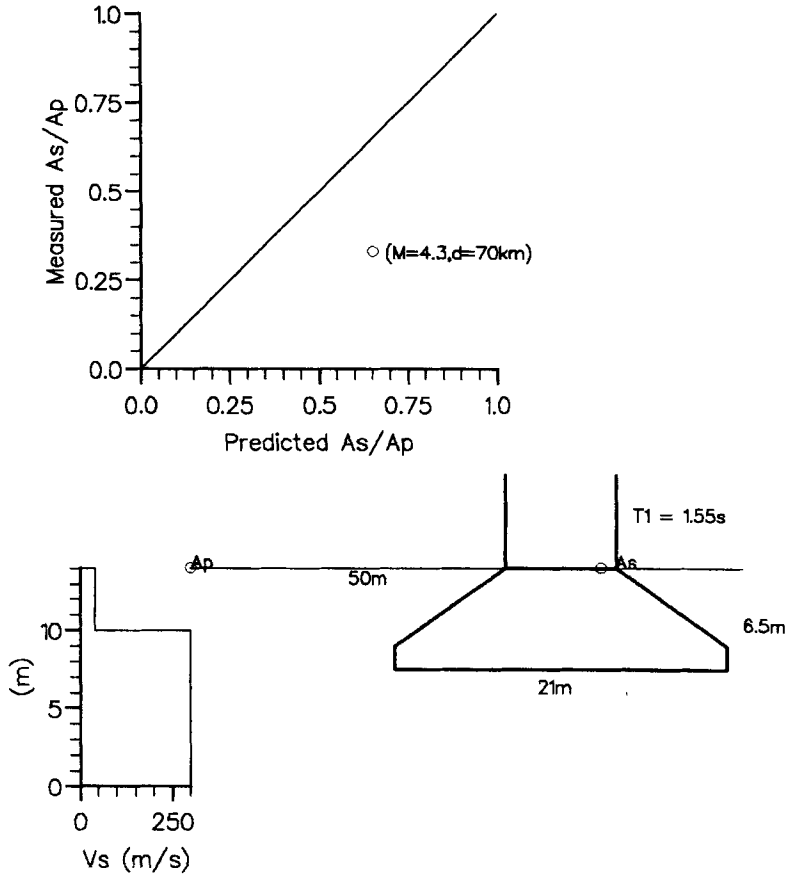

Figure 9. Relevant data for case 3: elevator tower at Mito

CONCLUSIONS

The simplified method can be used for the estimation of peak acceleration at the centre of the rigid and relatively lightweight foundation located near the ground surface when the foundation mass is uniformly distributed and the foundation will not slide on its base. It can also be used to check the need for implementation of a more sophisticated method. There are several factors that can influence the results of the simplified method proposed here and the designer should be aware of them. These factors are the embedment of foundation, the rotational acceleration, the flexibility of the foundation, the sliding of foundation, the non-uniform distribution of foundation mass and the inertial soil–structure interaction, which are not considered by the method. However, the prediction by the simplified method is based on a minimal number of key parameters that can be determined or predicted using established techniques and accepted procedures.

ACKNOWLEDGEMENTS

This work was supported by the European Council Environment Research Programme, contract EVSV-CT94-0490 Climatology and Natural Hazards, DG XII, Bruxelles. The ideas, data and the constructive comments made by Professor Ambraseys are gratefully acknowledged.

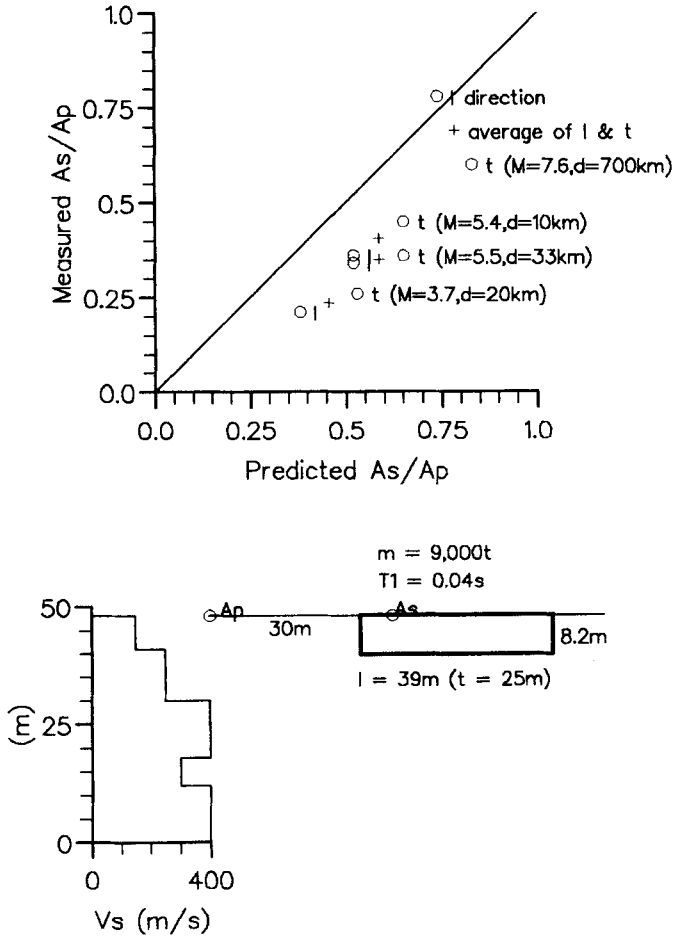

Figure 10. Relevant data for case 4: shaking table at National Research Center for Disaster Prevention Agency

APPENDIX I

Acceleration eccentricity

Eetemaadi[20] derived an expression for the rotational moment around the centre of a rigid foundation of the resultant seismic force. The expression for the eccentricity e_t at time t of resultant acceleration $L_s a_{s,t}$ with respect to the foundation centre and in the case when there is no relative displacement between the foundation and the ground as well as when the foundation mass is uniformly distributed is

$$\begin{aligned} e_t &= \frac{1}{L_s a_{s,t}}\left[\int_{L-L_s}^{L} a_l l \, dl - L_s a_{s,t}(L - 0{\cdot}5L_s)\right] \\ &= \frac{V_s^2}{L_s a_{s,t}}\left[\int_{t-T_s}^{t} a_t t \, dt - (v_t - v_{t-T_s})(t - 0{\cdot}5T_s)\right] \\ &= \frac{V_s^2}{L_s a_{s,t}}[0.5T_s(v_t + v_{t-T_s}) - d_t + d_{t-T_s}] \end{aligned} \tag{12}$$

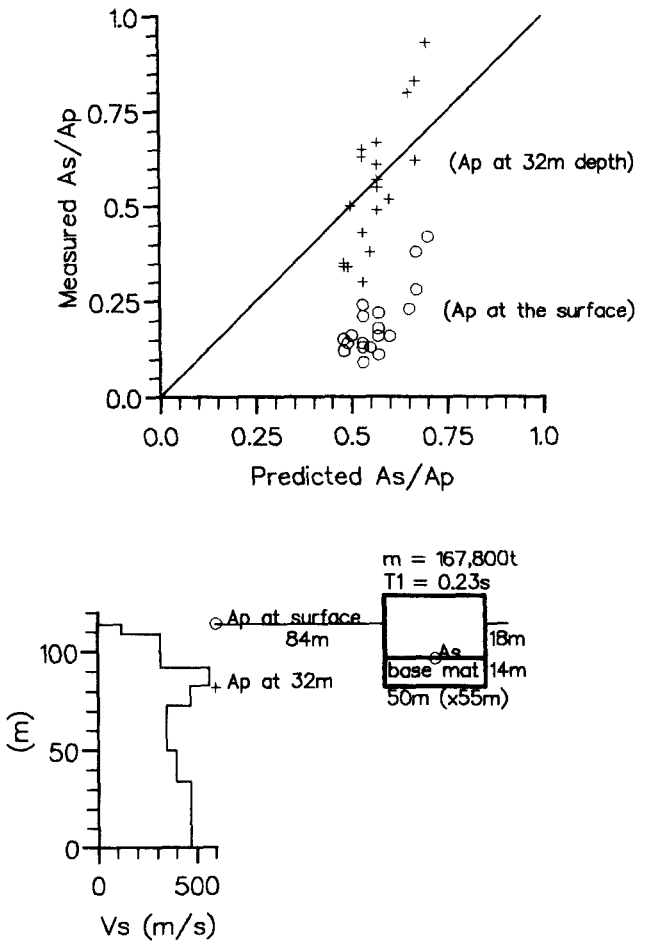

Figure 11. Relevant data for case 5: reactor building 'JOYO'

The eccentricity e_t can be normalized with respect to a half of foundation length $0{\cdot}5L_s$,

$$\frac{e_t}{0{\cdot}5L_s} = \frac{2}{T_s(v_t - v_{t-T_s})}[0{\cdot}5T_s(v_t + v_{t-T_s}) - d_t + d_{t-T_s}] \tag{13}$$

Near the beginning of acceleration record when $t < T_s$

$$\frac{e_t}{0{\cdot}5L_s} = \frac{2}{T_s(v_t - v_0)}[0{\cdot}5T_s v_t + (t - 0{\cdot}5T_s)v_0 - d_t + d_0] \tag{14}$$

Near the end of acceleration record when $t > t_{end}$

$$\frac{e_t}{0{\cdot}5L_s} = \frac{2}{T_s(v_{end} - v_{t-T_s})}[0{\cdot}5T_s v_{t-T_s} + (t_{end} - t + 0{\cdot}5T_s)v_{end} - d_{end} + d_{t-T_s}] \tag{15}$$

where d_t, d_{t-T_s} are the ground displacements at times t and $t - T_s$, d_0 is the initial ground displacement and d_{end} is the final ground displacement.

Equations (12)–(15) contain values of ground displacement, which are obtained by double integration of processed ground acceleration in time, and are much more affected by the applied processing procedure than

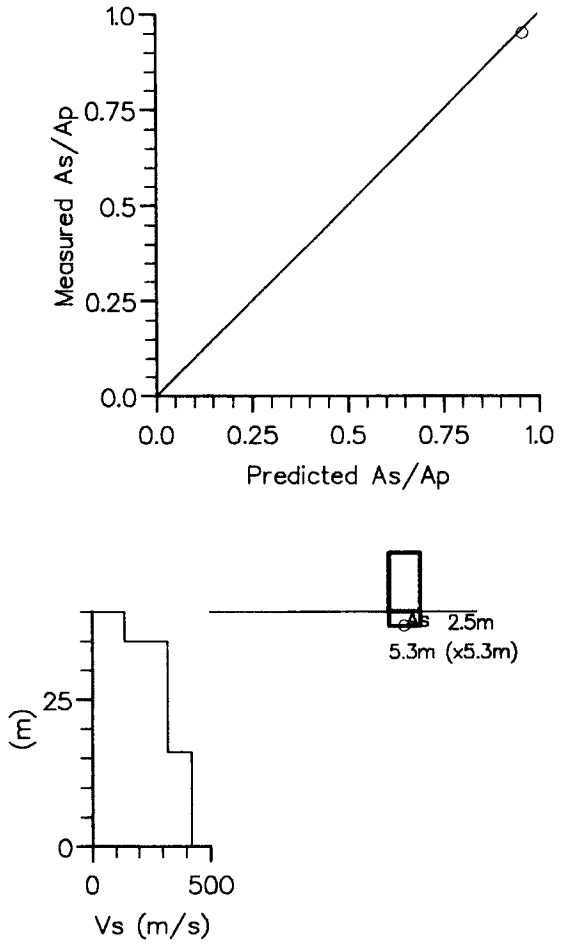

Figure 12. Relevant data for case 6: observation tower at Chiba Experiment Station

the ground velocity. The average value of the ratio between e_t and $0{\cdot}5L_s$, when the peak footing acceleration A_s is acting, is in the range from 0·1 to 0·3 for square footings and in the range from 0·01 to 0·15 for strip footings for the range of T_s between 0·04 and 0·5 s. A rather large standard deviation of about 3·8 times makes it difficult to predict this ratio with some confidence.

APPENDIX II

Case histories

Case 1: Valera *et al.*[21] considered seismic soil–structure interaction effects at Humboldt Bay Power Plant during the Ferndale earthquake of 7 June 1975. Although the duration of strong shaking was only about 3–5 s, the corrected peak accelerations developed in the free field (storage building) were $0{\cdot}35g$ and $0{\cdot}26g$ in the horizontal directions. The shear wave velocity of the soils at the site has not been measured but calculated from the value of dynamic shear moduli, which were determined by standard soil testing procedures using resonant column and cyclic triaxial tests on undisturbed samples reconsolidated under the *in situ* confining pressures. The input data and the results obtained using the simplified method are shown in Figure 7. The ratios of measured and predicted A_s and A_p are in excellent agreement for accelerograph B located in the building at the ground level. For accelerograph A located on the foundation at a depth of 26 m the ratio of

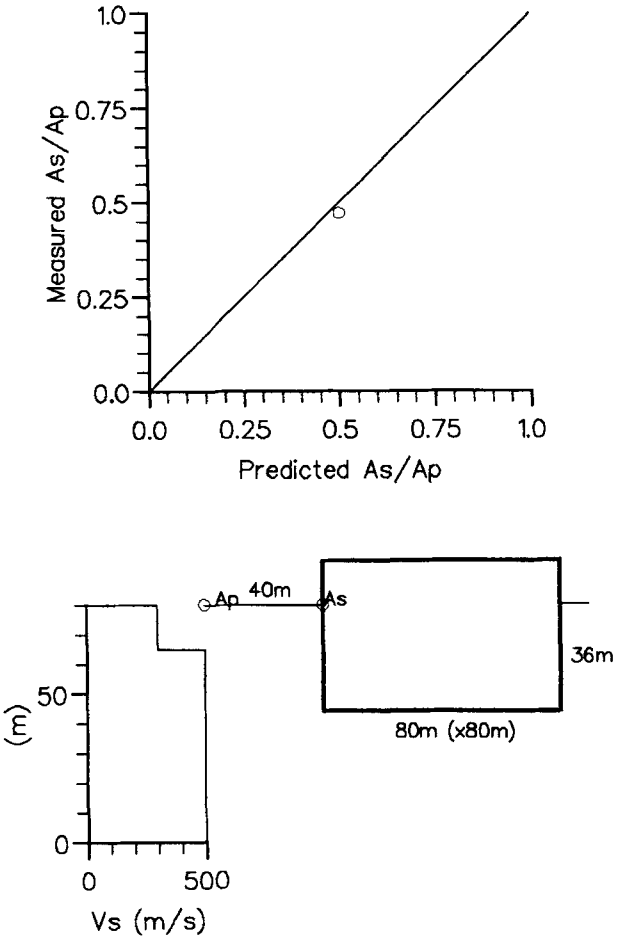

Figure 13. Relevant data for case 7: reactor building

predicted accelerations is larger than the ratio of measured accelerations, most probably as a result of larger A_p measured at the surface than it would be at the depth of 26 m in free field.

Case 2: Hirashima *et al.*[22] described observations and analysis of behaviour of a large foundation mat during the earthquake recorded at Tokai No. 2 Nuclear Power Plant. The input data and the results of application of the simplified method are shown in Figure 8. Good agreement between ratios for measured and predicted A_s and A_p would have been obtained if the accelerograph in the free field was located at the level of the accelerograph on the foundation. For the accelerograph located at a greater depth the simplified method underpredicted the ratio while for the accelerograph at the ground surface the method overpredicted the ratio due to the effect of foundation embedment and the change of peak ground acceleration with depth in the free field.

Case 3: Kishida *et al.*[23] reported on the results of forced vibration tests and recordings of earthquake accelerations measured in the free field and on a mat foundation supporting an 80 m high steel tower in Mito city. The shear wave velocity through the gravel below the foundation has not been measured but calculated from the results of SPT N value using the equation suggested by Ohta and Goto referred to by Seed *et al.*[24] Figure 9 shows the input data and the ratios between A_s and A_p measured and predicted using the simplified method. The method overpredicted the ratio probably as a result of the influence of rotational acceleration on the translational component recorded by the instrument, which was located at the edge instead of in the

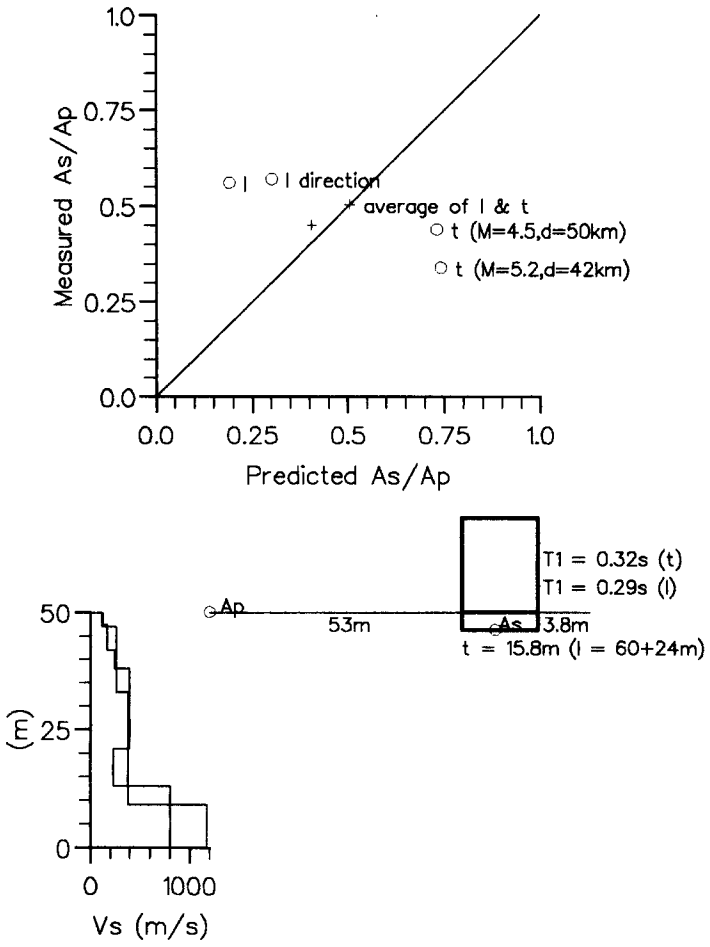

Figure 14. Relevant data for case 8: Earthquake Research Institute main building

centre, or due to the effect of inertial soil–structure interaction, which is not considered by the simplified method. The effect of rotational acceleration on the translational component is difficult to predict due to the large standard deviation.

Case 4: Tajimi *et al.*[25] described the results of investigations of the dynamic response of the foundation of a large shaking table and its surrounding ground during forced vibration tests and a number of earthquakes. Figure 10 shows the input data and the results of measurements and predictions using the simplified method. The method overpredicted the ratio between A_s and A_p in almost all cases regardless of earthquake magnitudes and source to side distances. The results indicate that the ratio is larger for earthquakes with greater magnitudes but it is not distance dependent. This finding is in good agreement with the coefficients in the predictive equations (5) and (11). Also the ratios were different for the longitudinal and transverse sides of the foundation (with peak accelerations in transverse and longitudinal directions, respectively). This may be because of the influence of rotational acceleration on the translational component in the transversal direction measured at the instrument located away from the centre of the foundation.

Case 5: Yajima *et al.*[26] summarized the results of observations of ground and foundation acceleration at the reactor building JOYO measured during a number of earthquakes. Data about shear wave velocities through the ground at the site were reported by Ueshima *et al.*[27] Figure 11 shows relevant data. As in the cases 1 and 2, better agreements between measurements and predictions were achieved when peak ground

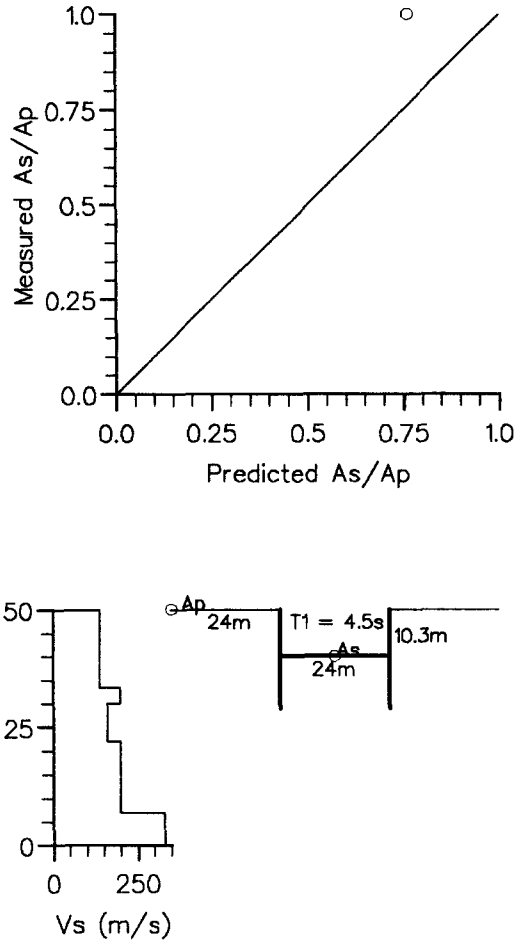

Figure 15. Relevant data for case 9: reinforced concrete underground tank

accelerations were measured at greater depth than at the surface due to embedment effects on the deep mat foundation. Also as in case 4, the earthquakes with greater magnitudes induced and have predicted greater $A_s A_p^{-1}$ ratios than the earthquakes of smaller magnitudes irrespective of source to site distance.

Case 6: Yamagami and Hangai[28] examined the response behaviour of a reinforced concrete tower during two earthquakes. They identified both material and geometrical non-linear behaviour caused by the separation of the structure from the ground. Figure 12 shows relevant data. Both measured and predicted ratios of A_s and A_p are the same and almost equal to 1 due to the small dimensions of the foundation.

Case 7: Hirota *et al.*[29] measured the earth pressure and acceleration of the structure and the surrounding soil at the site of a nuclear power plant. Figure 13 shows the input data and the results. The agreement between predicted and measured acceleration ratio is perfect but it may be as well coincidental.

Case 8: Osawa *et al.*[30,31] reported on the results of forced vibration tests and the measurements of strains, relative displacements, earth pressures and accelerations in a six-storey reinforced concrete building and its surrounding soil during strong earthquakes. They also considered soil–structure interaction effects using a one-dimensional wave propagation model, two-dimensional finite elements and a single mass ground compliance model in the frequency domain. It has been observed during forced vibration tests that rotational vibration is predominant in the transversal direction. The shear wave velocities through subsoil layers have been determined twice by explosion tests. The input data and the ratios between measured and predicted

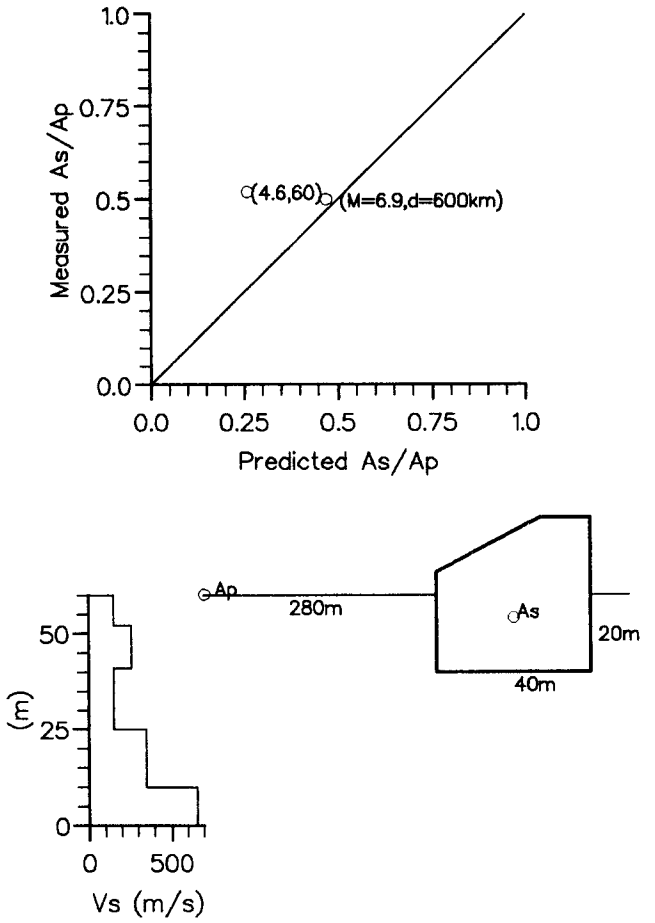

Figure 16. Relevant data for case 10: ventilation tower at first route of Tokyo Port Tunnel

A_s and A_p are shown in Figure 14. The simplified method underestimated the ratio for the longer building side (transversal peak acceleration) possibly as a result of insufficient rigidity of the superstructure and pad footings or the influence of rotational acceleration on the translational component recorded by the accelerometer located halfway between the centre and the end of building. On the contrary, the ratio is overpredicted for the shorter building side (longitudinal peak acceleration) although the instrument was located along the centre line in the longitudinal direction and may be the result of an inertial soil–structure interaction, which is not considered by the method. The prediction using the simplified method is excellent for the average building size and both earthquakes considered.

Case 9: Hamada and Sato[32] conducted observations of the behaviour of an underground tank during an earthquake. The bottom slab of the tank is only 20 cm thick. The dominant period of vibration of 4·5 s was considered to be caused by the vibration of the water in the tank. Figure 15 contains relevant data. The simplified method underestimated the $A_s A_p^{-1}$ ratio in comparison with measured accelerations probably as a result of insufficient rigidity of the foundation.

Case 10: Hamada *et al.*[33] performed observations during two earthquakes in order to clarify dynamic behaviour and the interaction between surrounding ground and a submerged tunnel incorporating a ventilation tower. The shear wave velocity of soil was adopted by the authors on the basis of measurements at the shore. Figure 16 shows relevant data for the ventilation tower. The accelerations recorded in the tunnel segments were similar to those of the ground in the longitudinal and transverse directions. The

underprediction of the ratio between A_s and A_p may be because of the adopted value of shear wave velocity. Again, as before, the predicted ratio is greater for earthquakes with greater magnitude regardless of source to site distance.

REFERENCES

1. H. Yamahara, 'Ground motions during earthquakes and the input loss of earthquake power to an excitation of buildings', *Soils found.* **10**, 145–161 (1970).
2. J. N. Brune, 'Foam rubber modelling of the El Centro Terminal Substation Building', *Earthquake spectra* **7**, 45–77 (1991).
3. V. W. Lee, M. D. Trifunac and C. C. Feng, 'Effects of foundation size on fourier spectrum amplitudes of earthquake accelerations recorded in buildings', *Soil dyn earthquake eng.* **1**, 52–58 (1982).
4. P. J. Hradilek, A. R. Carriveau, G. R. Sargoni and C. M. Duke, 'Evidence of soil–structure interaction in earthquakes', *Proc. 5th world conf. earthq. eng.* (Rome) **5**, 2076–2079 (1974).
5. N. M. Newmark, 'Torsion in symmetrical buildings', *Proc. 4th world conf. earthquake eng.* (Santiago de Chile) **2**, 19–32 (1969).
6. H. L. Wong and J. E. Luco, 'Dynamic response of rectangular foundations to obliquely incident seismic waves', *Earthquake eng. struct. dyn.* **6**, 3–16 (1978).
7. R. H. Scanlan, 'Seismic wave effects on soil–structure interaction', *Earthquake eng. struct. dyn.* **4**, 379–388 (1976).
8. M. Hoshiya and K. Ishii, 'Evaluation of kinematic interaction of soil–foundation systems by a stochastic model', *Soil dyn. earthquake eng.* **2**, 128–134 (1983).
9. N. M. Newmark, 'Design criteria for nuclear reactors subjected to earthquake hazards', *Proc. IAEA panel on aseismic design and testing of nuclear facilities*, Japan Earthquake Eng. Promotion Society, Tokyo, 1967.
10. S. K. Sarma and K. S. Yang, 'An evaluation of strong motion records and a new parameter A_{95}', *Earthquake eng. struct. dyn.* **15**, 119–132 (1987).
11. N. M. Newmark, W. J. Hall and J. R. Morgan, 'Comparison of building response and free field motion in earthquakes', *Proc. 6th world conf. earthquake eng.* (New Delhi) **2**, 972–977 (1977).
12. J. M. H. Menu, 'Engineering study of near field earthquake strong motions', *Ph.D. thesis*, University of London, U.K., 1986.
13. W. B. Joyner and D. M. Boore, 'Peak horizontal acceleration and velocity from strong motion records including records from the 1979 Imperial Valley, California, earthquake', *Bull. seism. soc. Amer.* **71**, 2011–2038 (1981).
14. N. N. Ambraseys, 'The prediction of earthquake peak ground acceleration in Europe', *Earthquake eng. struct. dyn.* **24**, 467–490 (1995).
15. W. B. Joyner and D. M. Boore, 'Prediction of earthquake response spectra', *Proc. 51st ann. convention struct. eng. assoc. of California, also U.S. Geol. Surv. Open File Report*, 82-977, 16p, 1982.
16. N. N. Ambraseys, K. Simpson and J. J. Bommer, 'Prediction of horizontal response spectra in Europe', *Earthquake eng. struct. dyn.* **25**, 371–400 (1996).
17. K. W. Campbell, (1988). Cited by W. B. Joyner and D. M. Boore in 'measurement, characterization, and prediction of strong ground motion', *Proc. earthquake engineering soil dynamics* 2, *GT Div. ASCE* 43–102 (1988).
18. K. Kawashima, K. Aizawa and K. Tahakashi, 'Attenuation of peak ground motion and absolute acceleration response spectra', *Proc. 8th world conf. earthquake engin.* (San Francisco) **2**, 257–264 (1984).
19. N. N. Ambraseys and M. Srbulov, 'Attenuation of earthquake induced ground displacements', *Earthquake eng. struct. dyn.* **23**, 467–487 (1995).
20. M. I. Eetemaadi, 'Foundation effects on free field strong ground motions', *Ph.D. thesis*, University of London, U.K., 1980.
21. J. E. Valera, H. B. Seed, C. F. Tsai and J. Lysmer, 'Seismic soil–structure interaction effects at Humboldt Bay Power Plant', *J. geotech. eng. div. ASCE* **103**, 1143–1161 (1977).
22. S. Hirashima, M. Kato and T. Ueshima, 'Earthquake observations and analysis of a nuclear power plant', *Proc. 7th world conf. earthquake eng.* (Istanbul) **8**, 17–25 (1980).
23. H. Kishida, K. Matsushita and I. Sakamoto, 'Soil–structure interaction of the elevator tower and of concrete footings', *Proc. 4th world conf. earthquake eng.* (Santiago de Chile) **3**, 101–115 (1969).
24. H. B. Seed, R. T. Wong, I. M. Idriss and K. Tokimatsu, 'Moduli and damping factors for dynamic analyses of cohesionless soils', *J. geotech. eng. ASCE* **112**, 1016–1032 (1986).
25. H. Tajimi, C. Minowa and Y. Shimomura, 'Dynamic response of a large-scale shaking table foundation and its surrounding ground', *Proc. 6th world conf. earthquake eng.* (New Delhi) **2**, 1516–1521 (1977).
26. H. Yajima, Y. Sawada, K. Hanada and M. Sawada, 'Earthquake response characteristics of large structure "JOYO" deeply embedded in Quaternary ground', *Strong motion array observation* **1**, 101–124 (1993).
27. T. Ueshima, Y. Sawada, H. Yajima, K. Ohtomo and M. Sawada, 'Dynamic characteristics of large structure "JOYO" deeply embedded in Quaternary ground and evaluation of embedment effect', *Proc. 9th world conf. earthquake eng.* (Tokyo) **3**, 739–744 (1988).
28. T. Yamagami and Y. Hangai, 'Response observation of a reinforced concrete tower', *Proc. 9th world conf. earthquake eng.* (Tokyo) **3**, 715– 720 (1988).
29. M. Hirota, M. Sugimoto and S. Onimaru, 'Study on dynamic earth pressure through observation', *Proc. 10th world conf. earthquake eng.* (Madrid) **3**, 1735–1739 (1992).
30. Y. Osawa, T. Tanaka, M. Murakami and Y. Kitagawa, 'Earthquake measurements in and around a reinforced concrete building', *Proc. 4th world conf. earthquake eng.* (Santiago de Chile) **1**, 1–16 (1969).
31. Y. Osawa, Y. Kitagawa and K. Ishida, 'Response analyses of earthquake motions observed in and around a reinforced concrete building including building-subsoil system', *Proc. 5th world conf. earthquake eng.* (Rome) **2**, 1891–1900 (1974).
32. M. Hamada and S. Sato, 'Behaviour of underground tank during earthquakes', *Proc. 6th world conf. earthquake eng.* (New Delhi) **2**, 1503–1507 (1977).
33. M. Hamada, T. Akimoto and H. Izumi, 'Dynamic stress of a submerged tunnel during earthquakes', *Proc. 6th world conf. earthquake eng.* (New Delhi) **2**, 1509–1515 (1977).